Transition Met Chem (2010) 35:605–611
DOI 10.1007/s11243-010-9370-1

Synthesis, characterization, photophysical and oxygen-sensing properties of a copper(I) complex

Chuanqi Zhou · Qingshuang Wang

Received: 22 January 2010 / Accepted: 7 May 2010 / Published online: 26 May 2010

Abstract In this paper, we report the synthesis, crystal structure, photophysical properties, and electronic nature of a phosphorescent Cu(I) complex of [Cu(TBT)(POP)]BF_4, where TBT and POP stand for 4,5,9,14-tetraaza-benzo[b]-triphenylene and bis(2-(diphenylphosphanyl)phenyl) ether, respectively. [Cu(TBT)(POP)]BF_4 renders a red phosphorescence peaking at 622 nm, with a long excited-state lifetime of 13.2 μs. Density functional calculation reveals that the emission comes from a triplet metal-to-ligand-charge-transfer excited state. We electrospun composite nanofibers of [Cu(TBT)(POP)]BF_4 and polystyrene, hoping to explore the possibility of replacing precious-metal-based oxygen sensors with cheap Cu-based ones. The finally obtained samples with average diameter of ~700 nm exhibit a maximum sensitivity of 5.8 toward molecular oxygen with short response/recovery time (5/13 s) due to the large surface-area-to-volume ratio of nanofibrous membranes. No photobleaching is detected in these samples. All these results suggest that phosphorescent Cu(I) complexes doped nanofibrous membranes are promising candidates for low-cost and quick-response oxygen-sensing materials.

Electronic supplementary material The online version of this article (doi:10.1007/s11243-010-9370-1) contains supplementary material, which is available to authorized users.

C. Zhou (✉)
Beijing Institute of Genomics, Chinese Academy of Sciences, No. 7 Beitucheng West Road, Chaoyang District, 100029 Beijing, People's Republic of China
e-mail: chuanqizhou@gmail.com

Q. Wang
School of Life Science and Technology, Changchun University of Science and Technology, 7089 Weixing Road, Changchun, 130022 Jilin, People's Republic of China

Introduction

During the past decade, a great interest in transition metal complexes, especially heavy metal complexes such as Ru(II) and Re(I) complexes, has been sparked by the development of practical components for chemical sensors, display devices, biological probes, phototherapy, and solar-energy conversion [1, 2]. At the same time, strong appeal of replacing the expensive compounds based on precious metal complexes with cheap ones, as well as the need for a deeper understanding on the correlation between molecular structures and photophysical properties, has pushed a continuous progress in the design of luminescent first-row transition metal complexes. Phosphorescent Cu(I) complexes, as a new class of optoelectrical material, have drawn much attention due to their advantages of lower toxicity, low cost, abundant resource, and environmental friendliness [3].

Generally, emission signals from charge-transfer excited states of copper(I) complexes are typically weak and short lived because the lowest energy charge-transfer state of a d^{10} system involves excitation from a metal–ligand dσ^* orbital [3, 4]. An important consequence is that the excited state typically prefers a tetragonally flattened geometry, whereas the ground state usually adopts a tetrahedral-like coordination geometry appropriate for a closed-shell structure. Aside from reducing energy content, the geometric relaxation that occurs in excited states facilitates relaxation back to the ground state [5, 6]. McMillin, Cuttell, Walton, and coworkers first reported this type of exciplex quenching, and by now, many other studies have confirmed the mechanism [3, 7, 8].

Mixed-ligand systems involving triphenylphosphane seem to be promising because they exhibit long excited-state lifetimes in solid state and frozen solutions [9, 10].

A series of new mixed-ligand copper(I) complexes such as $[Cu(N–N)(POP)]^+$ [POP=bis(2-(diphenylphosphanyl)-phenyl) ether] which are superior emitters have been synthesized. It is found that the exciplex quenching is relatively inefficient for the charge-transfer excited state in this POP system. In addition, the introduction of sterically blocking ligands can impede geometric relaxation as well as solvent attack [11]. Here, steric effects cooperate to effectively constrain the excited state close to the ground-state geometry, which has been proved by the theoretical studies by Feng and coworkers on $[Cu(N–N)(P–P)]^+$ system [12]. For a typical phosphorescent Cu(I) complex, the highest occupied molecular orbital (HOMO) has a predominant metal Cu d character, while the lowest unoccupied orbital (LUMO) is essentially π^* orbitals localized on the diimine ligand. The photoluminescence corresponds to the lowest triplet T_1 and is thus assigned as a character of metal-to-ligand-charge-transfer ^{3}MLCT [d(Cu) $\rightarrow$ π^*(diimine ligand)]. The MLCT excited states of cuprous diimine compounds are often luminescent and play important roles in photoinduced electron and energy transfer process.

In this paper, we report a phosphorescent Cu(I) complex, namely $[Cu(TBT)(POP)]BF_4$, where TBT stands for 4,5,9,14-tetraaza-benzo[b]triphenylene. Its crystal structure, photophysical properties, and electronic nature are discussed in detail. In addition, we electrospun composite nanofibers of $[Cu(TBT)(POP)]BF_4$/polystyrene, hoping to explore the possibility of replacing precious-metal-based oxygen sensors with cheap Cu-based ones. The resulting samples exhibit a maximum sensitivity of 5.8 toward molecular oxygen with short response/recovery time (5/13 s), and no photobleaching is detected in these samples.

Experimental section

A synthetic route for the diimine ligand of TBT and its corresponding Cu(I) complex with POP as the auxiliary ligand is shown in Scheme 1. Bis[2-(diphenylphosphino)-phenyl] ether (POP, 99% purity), $Cu(BF_4)_2$ (AR grade), 1,10-phenanthroline (AR grade), benzene-1,2-diamine (AR grade), and polystyrene (melt flow rate = 3.4 g/10 min) were purchased from Aldrich Chemical Co. and used without further purifications. Organic solvents were purified through standard procedures. 1,10-phenanthroline-5,6-dione and $[Cu(CH_3CN)_4]BF_4$ was synthesized according to the literature procedures [11, 13].

Synthesis of the diimine ligand

4,5,9,14-tetraaza-benzo[b]triphenylene (TBT) was synthesized by a modification of a literature method [14]. A mixture of 5 mmol of 1,10-phenanthroline-5,6-dione, 5.5 mmol of benzene-1,2-diamine, 25 mL of ethanol, and 0.05 mmol of 4-methylbenzenesulfonic acid was heated at 80 °C for 10 h, the crude product was filtered off and then recrystallized from ethanol to give the pure desired product. Yield 1.11 g (79%). ^{1}H NMR (300 Hz, $CDCl_3$, 25 °C): δ 9.63(d, 2H, J = 8.0 Hz), 9.21(d, 2H, J = 8.0 Hz), 8.37(d, 2H, J = 6.4 Hz), 7.87(d, 2H, J = 6.4 Hz), 7.78(m, 2H). Anal. Calcd. for $C_{18}H_{10}N_4$: C, 76.60; H, 3.55; N, 19.86. Found: C, 76.71; H, 3.67; N, 19.72.

Synthesis of the Cu(I) complex

$[Cu(TBT)(POP)]BF_4$ was synthesized according the literature procedures except that the diimine was replaced by TBT [7, 11]. Its identity was confirmed by NMR, elemental analysis, and single-crystal XRD (CCDC 731780 which can be obtained free of charge from The Cabridge Crystallographic Data Center via www.ccdc.cam.ac.uk/data_request/cif, please also see Supplementary Material for crystal data). ^{1}H NMR (300 Hz, $CDCl_3$, 25 °C): δ 9.61(d, 2H, J = 8.0 Hz), 9.25(d, 2H, J = 8.0 Hz), 8.31(d, 2H, J = 6.4 Hz), 7.92–7.77(m, 22H), 7.35–7.31(m, 10H). Anal. Calcd. for $C_{54}H_{38}BCuF_4N_4OP_2$: C, 66.78; H, 3.94; N, 5.77. Found: C, 66.70; H, 3.81; N, 5.81.

Fabrication of $[Cu(TBT)(POP)]BF_4$/polystyrene nanofibrous membranes

A typical procedure for the electrospinning of composite nanofibers is described as follows. Polystyrene with a number-average molecular mass of 100,000 was dissolved in *N*,*N*′-dimethyl formamide (DMF) to form a 22 wt% solution. Then $[Cu(TBT)(POP)]BF_4$ was added into the solution under stirring to form $[Cu(TBT)(POP)]BF_4$/polystyrene homogeneous solutions. The final solutions were then electrospun to give composite nanofibrous membranes of $[Cu(TBT)(POP)]BF_4$/polystyrene.

Methods and measurements

Density functional theory (DFT) and singlet excitation calculations using time-dependent density functional theory (TD-DFT) were performed on $[Cu(TBT)(POP)]^+$ at RB3LYP/SBKJC level. The initial geometry was obtained from its single crystal. All computations were done with the GAMESS software package. Excited-state lifetimes were obtained with a 355-nm light generated from the Third-Harmonic-Generator pumped, using pulsed Nd:YAG laser as the excitation source. The Nd:YAG laser possesses a line width of 1.0 cm^{-1}, pulse duration of 10 ns and repetition frequency of 10 Hz. A Rhodamine 6G dye pumped by the same Nd:YAG laser was used as the frequency-selective excitation source. All photoluminescence

Scheme 1 A synthetic route for TBT and [Cu(TBT)(POP)]BF_4

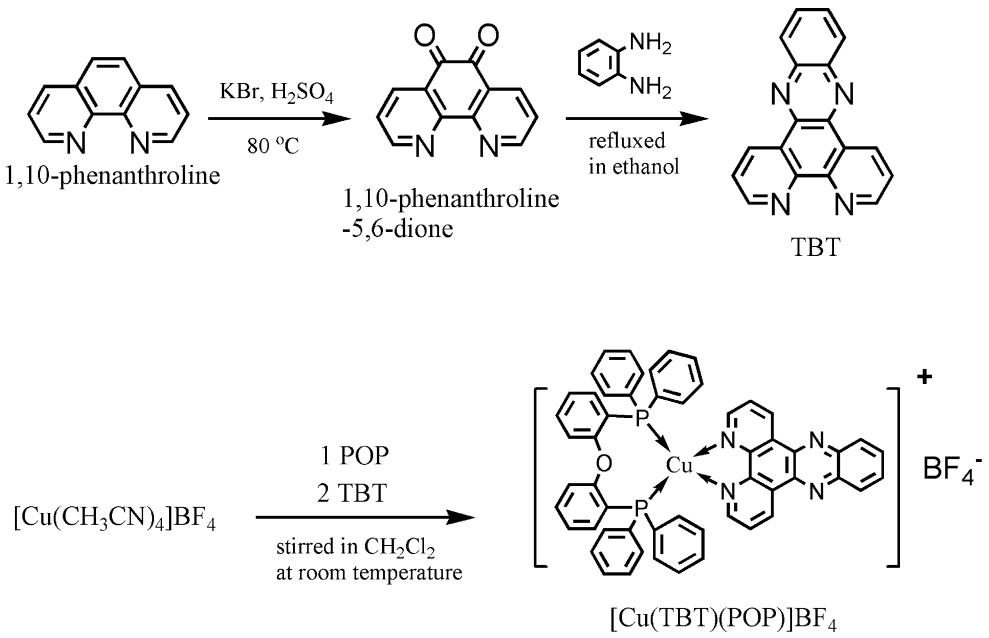

(PL) spectra were measured with a Hitachi F-4500 fluorescence spectrophotometer. UV–Vis absorption spectra were recorded using a Shimadzu UV-3101PC spectrophotometer. Scanning electron microscopy (SEM) images were obtained on a Hitachi S-4800 microscope. ^{1}H NMR spectra were obtained with a Varian INOVA 300 spectrometer. Elemental analysis was performed on a Carlo Erba 1106 elemental analyzer. Single-crystal data were collected on a Siemens P4 single-crystal X-ray diffractometer with a Smart CCD-1000 detector and graphite-monochromated Mo Kα radiation, operating at 50 kV and 30 A at 298 K. All hydrogen atoms were calculated. Oxygen-sensing performances were measured on the basis of steady emission intensity quenching. All measurements were carried out in the air at room temperature without being specified.

Results and discussion

Crystal structure of [Cu(TBT)(POP)]BF_4

Figure 1 shows the molecular structure of [Cu(TBT)(POP)]-BF_4 obtained from its single crystal. Geometric parameters listed in Table 1 suggest that the Cu(I) center has a distorted tetrahedral coordination sphere. The dihedral angle between N–Cu–N and P–Cu–P planes is 89.6°. Cu–N bond lengths in [Cu(TBT)(POP)]BF_4 occupy a narrow region of 2.05–2.06 Å which are comparable to literature values [5, 6, 11, 12]. Similarly, the two Cu–P bond lengths are exactly the same with a distance of 2.24 Å away from the Cu(I) center. The O atom of the POP ligand lies at a distance of ~3 Å away from the Cu(I) center and opposite to the coordinated N atoms, indicating a weak interaction between O atom and Cu(I) center. Similar Cu···O separations have also been reported in POP-based Cu(I) complexes that contain 1,10-phenanthroline derived ligands, which means that the Cu(I) center tends to achieve a five-coordinated environment [5, 6, 11, 12].

Unlike the literature values of ~80°, the N–Cu–N bond angle of [Cu(TBT)(POP)]BF_4 (81.2°) is somewhat greater, clearly due to the reduced static congestion caused by the large dihedral angle between N–Cu–N and P–Cu–P planes of [Cu(TBT)(POP)]BF_4 (89.58°) as mentioned [11, 12]. On the other hand, the P–Cu–P bond angle is as large as 113.2°, as shown in Table 1. Considering POP's natural bite angle of 102.2°, with a flexibility range from 86° to 120°, the large P–Cu–P bond angle in [Cu(TBT)(POP)]BF_4

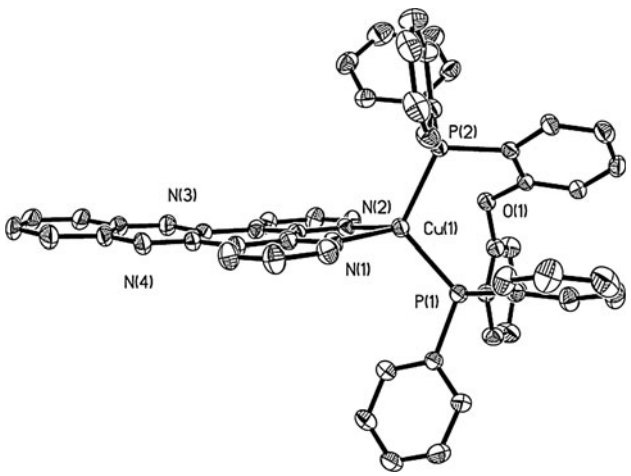

Fig. 1 Molecular structure [Cu(TBT)(POP)]BF_4 obtained from its single crystal. BF_4^- moiety and all hydrogen atoms are omitted for clarity

Table 1 Selected geometric parameters of $[Cu(TBT)(POP)]BF_4$ obtained from single-crystal data

Bond length	Å	Bond angle	°
Cu(1)–N(1)	2.051(5)	N(1)–Cu–N(2)	81.20(2)
Cu(1)–N(2)	2.062(5)	N(1)–Cu–P(1)	117.21(15)
Cu(1)–P(1)	2.2421(18)	N(2)–Cu–P(1)	112.82(14)
Cu(1)–P(2)	2.2435(18)	N(1)–Cu–P(2)	116.71(14)
Cu···O	3.08	N(2)–Cu–P(2)	111.51(14)
		P(1)–Cu–P(2)	113.26(7)

suggests a crowded coordination environment around the Cu(I) center. Correspondingly, N–Cu–N and P–Cu–P planes tend to spread out to minimize the crowed environment [15].

Photophysical properties of $[Cu(TBT)(POP)]BF_4$

Figure 2 shows the UV–Vis absorption spectrum of $[Cu(TBT)(POP)]BF_4$ in CH_2Cl_2 solution with a concentration of 1×10^{-4} mol/L, along with those of TBT and POP ligands. The $[Cu(TBT)(POP)]BF_4$ absorption spectrum is composed of a strong absorption band ranging from 250 to 330 nm and a weak low-energy absorption band ranging from 350 to 500 nm. From the comparison between those absorption spectra, the former absorption band should correspond to ligands $\pi \rightarrow \pi^*$ transitions, while the latter one is experimentally assigned as MLCT transition absorptions [14]. Compared with that of $[Cu(Phen)(POP)]BF_4$ (Phen=1,10-phenanthroline), it is observed that the MLCT absorption of $[Cu(TBT)(POP)]BF_4$ red shifts by ~50 nm, owing to the enlarged coplanar conjugation system in the TBT ligand [11].

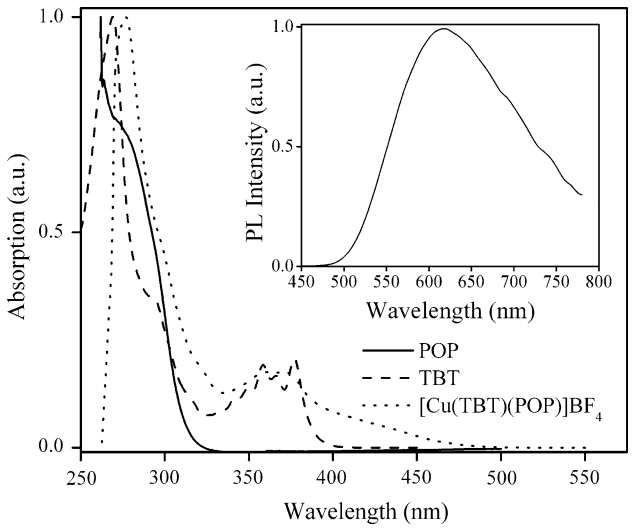

Fig. 2 UV–Vis absorption of TBT, POP, and $[Cu(TBT)(POP)]BF_4$ in CH_2Cl_2 solutions with a concentration of 1×10^{-4} mol/L. *Inset*: PL spectrum of $[Cu(TBT)(POP)]BF_4$ doped in PMMA

As shown in Fig. 2, the $[Cu(TBT)(POP)]BF_4$ doped poly(methyl methacrylate) (PMMA) film (10 wt%) renders a broad emission band peaking at 620 nm, without giving any vibronic progressions, suggesting a charge-transfer emissive character. The emission owns a long excited-state lifetime of 13.2 μs, indicating the presence of a triplet state emissive character. The large Stokes shift between absorption and emission spectra of $[Cu(TBT)(POP)]BF_4$ (120 nm) reveals a severe geometric relaxation that occurs in the excited state. Similarly, the emission peak also demonstrates a red shift compared with that of $[Cu(Phen)(POP)]BF_4$ peaking at ~550 nm, confirming that $[Cu(TBT)(POP)]BF_4$ owns a narrower energy gap than that of $[Cu(Phen)(POP)]BF_4$ due to TBT's larger coplanar conjugation system [11].

Theoretical calculations on $[Cu(TBT)(POP)]^+$

As mentioned earlier, the MLCT excited states of cuprous diimine compounds are often luminescent and play important roles in photoinduced electron and energy transfer process. In order to get a further understanding on the electronic nature of $[Cu(TBT)(POP)]BF_4$, we performed a DFT/TD-DFT calculation, which has been proved to be a powerful tool to investigate electronic properties of transition metal complexes, on $[Cu(TBT)(POP)]^+$ at B3LYP/SBKJC level [12]. As shown by Fig. 3 and Table 2, the HOMO of $[Cu(TBT)(POP)]^+$ has an evident metal Cu character, admixed with large contributions from the phosphorous ligand, while its LUMO is essentially diimine ligand π^* orbitals of TBT. The calculated onset transition of $S_0 \rightarrow S_1$ corresponds to an electronic transition from HOMO to LUMO as shown by Table 3, and the onset excitation transition (510.66 nm) correlates quite well with the experimentally recorded absorption edge shown in Fig. 2 (502 nm). It is thus confirmed that the onset electronic transition of $[Cu(TBT)(POP)]BF_4$ is a MLCT one. According to Feng's report, the photoluminescence of $[Cu(N–N)(P–P)] \pm$ complexes corresponds to the lowest triplet T_1, which consists of the transition from HOMO to LUMO or LUMO + 1, and is thus assigned as having mixed character between MLCT [d(Cu) $\rightarrow \pi^*$(phen)] [12]. Correspondingly, the emissive state of $[Cu(TBT)(POP)]BF_4$ is also expected to be a MLCT one. Combined with the long excited-state lifetime as mentioned, we come to a conclusion that the red emission of $[Cu(TBT)(POP)]BF_4$ originates from ^{3}MLCT excited state, which is consistent with a previous report [12].

Oxygen-sensing properties of $[Cu(TBT)(POP)]BF_4$/polystyrene nanofibrous membranes

Considering the long excited-state lifetime of $[Cu(TBT)(POP)]BF_4$ which makes the excited $[Cu(TBT)(POP)]BF_4$

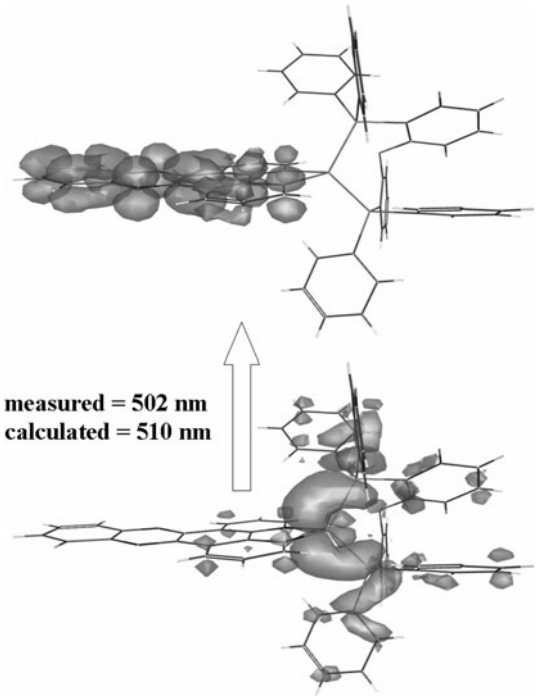

Fig. 3 LUMO (*up*) and HOMO (*down*) presentations of [Cu(TBT)-(POP)]$^+$ calculated at RB3LYP/SBKJC level with the contour value of 0.022

Table 2 Orbital percentage composition of [Cu(TBT)(POP)]$^+$ calculated at RB3LYP/SBKJC level

Orbitals	Composition (%)	Energy (eV)
LUMO + 1	TBT(81.2)	−4.34
LUMO	TBT(98.7)	−4.88
HOMO	Cu(24.1) POP(70.6)	−7.79
HOMO − 1	Cu(41.7) POP(20.1)	−8.15

molecule sensitive and vulnerable to any electron/energy acceptors, we intend to investigate its PL response toward oxygen and thus explore the possibility of replacing precious-metal-based oxygen sensors with cheap Cu-based ones. For practical applications in optical oxygen-sensing devices, it is necessary to embed the sensors into a solid matrix acting as a supporting medium, allowing oxygen transportation from the surroundings, and the support may also have quite stringent criteria for suitable performances. Here, we select polystyrene that has been proved to be an excellent host material for electrospinning as the supporting matrix for our earlier research [16, 17].

Morphology of [Cu(TBT)(POP)]BF_4/polystyrene nanofibrous membranes

To begin with, we tried four dopant concentrations of 1, 1.5, 2, and 2.5 wt%. The inset of Fig. 4 shows a typical SEM image of the 2 wt% doped sample. The composite fibers with average diameter of ~700 nm are randomly distributed on the substrate, showing a smooth and uniform morphology. No branch structure is observed for the composite fibers. Those composite fibers own a large surface-area-to-volume ratio which is two orders of magnitude larger than that of continuous thin films, providing an excellent matrix with high diffusion coefficient for a rapid response, which will be discussed later [18].

Sensitivity of [Cu(TBT)(POP)]BF_4/polystyrene nanofibrous membranes

Figure 4 shows the emission spectra of the 2 wt% doped sample under various oxygen concentrations from 0 to 100% with an interval of 10%. With increasing oxygen concentrations, the emission intensity at 560 nm decreases significantly. The sensitivity (I_0/I_{100}, where I_0 is the luminescence intensity under 100% N_2 atmosphere and I_{100} is that under 100% O_2 atmosphere) values of the four samples with various dopant concentrations are 5.1 for 1 wt% doped [Cu(TBT)(POP)]BF_4/polystyrene sample, 5.5 for 1.5 wt% doped [Cu(TBT)(POP)]BF_4/polystyrene sample, 5.8 for 2 wt% doped [Cu(TBT)(POP)]BF_4/polystyrene sample, and 4.4 2.5 wt% doped [Cu(TBT)(POP)]BF_4/polystyrene sample, respectively. Generally, a sensor with sensitivity higher than 3 can be used for actual applications, which means that all four samples are qualified enough to serve as actual sensors [19]. The 2 wt% doped sample exhibits a higher sensitivity than the others, which can be explained as follows. There may be at least two opposite factors affecting sample's sensitivity: emission intensity from probe molecules and adverse interaction between probe molecules (aggregation, for example). When the dopant concentration is low, emission from the probe is weak, leading to a low sensitivity. On the other hand, a much higher dopant concentration may accelerate the intermolecular aggregation which also decreases the sensitivity. The two opposite factors may achieve a balance in the 2 wt% doped sample, resulting in the maximum sensitivity of 5.8.

In addition, it is observed that the PL spectra of the 2 wt% doped sample, peaking at ~560 nm, exhibit a blue shift tendency compared with the PL spectrum of [Cu(TBT)(POP)]BF_4 centering at 620 nm. Correspondingly, the excited-state lifetimes of samples under 100% N_2 atmosphere are 100 μs for 1 wt% doped sample, 110 μs for 1.5 wt% doped sample, 120 μs for 2 wt% doped sample, and 90 μs for 2.5 wt% doped sample. The much longer excited-state lifetimes compared with that of pure [Cu(TBT)(POP)]BF_4 (13.2 μs) suggest a more stable emissive state, indicating that the geometric relaxation in excited state is largely and efficiently suppressed by the

Table 3 The first four singlet transitions of $[Cu(TBT)(POP)]^+$ calculated at RB3LYP/SBKJC level

Transitions	Composition (%)	Energy (nm)	Oscillator strength
$S_0 \rightarrow S_1$	HOMO → LUMO(95.9)	510.66	0.0038128
$S_0 \rightarrow S_2$	HOMO − 1 → LUMO(89.4)	456.13	0.0000309
$S_0 \rightarrow S_3$	HOMO − 1 → LUMO + 1(66.5)	436.75	0.0358045
	HOMO → LUMO + 1(24.3)		
$S_0 \rightarrow S_4$	HOMO → LUMO + 1(66.7)	429.86	0.1068919
	HOMO − 1 → LUMO + 1(25.1)		

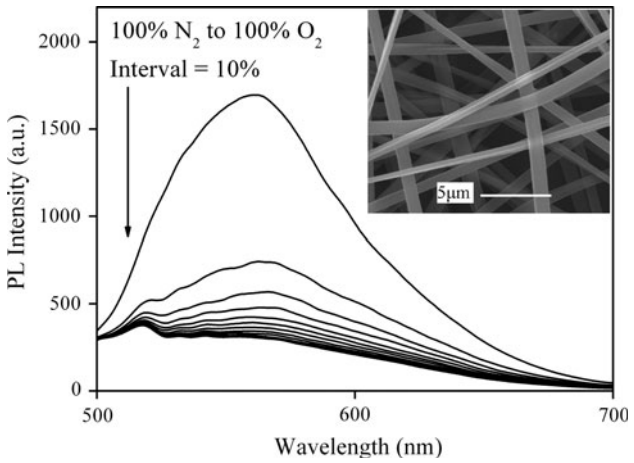

Fig. 4 Emission spectra of the 2 wt% doped sample under various oxygen concentrations from 0 to 100% with an interval of 10%. *Inset*: a SEM image of the 2 wt% doped sample

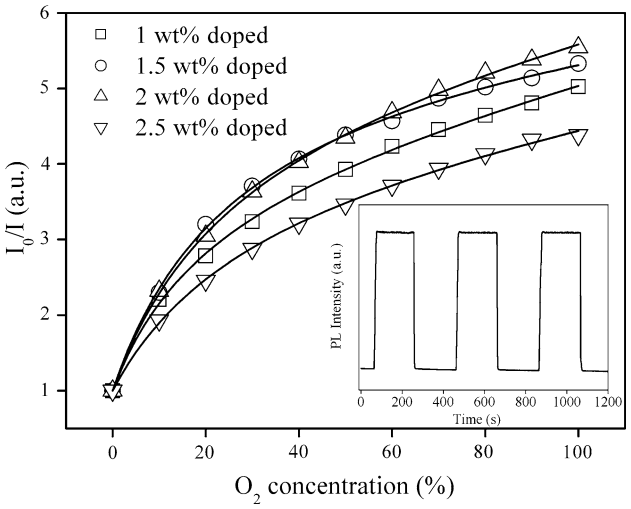

Fig. 5 Stern–Volmer plots of the four samples under various oxygen concentrations from 0 to 100% with an interval of 10%. *Solid lines* are fitted using nonlinear fitting method. *Inset*: PL intensity responses of the 2 wt% doped sample under periodically varied 100% N_2 and 100% O_2 atmospheres

rigid environment provided by polystyrene matrix. What's more, the 2.5 wt% doped sample's shorter excited-state lifetime compared with that of the 2 wt% doped sample confirms that a higher dopant concentration may accelerate the intermolecular aggregation as mentioned. On the other hand, compared to the sharp decrease at 620 nm, the emission at 517 nm seems to be more insensitive toward oxygen, suggesting its fluorescence nature. The ratio of fluorescence to total emission, however, is so small that the total emission is still highly sensitive toward oxygen.

Stern–Vomler plots of $[Cu(TBT)(POP)]BF_4$/polystyrene nanofibrous membranes

Figure 5 shows the Stern–Volmer plots of the four samples at various oxygen concentrations. Generally, in a homogeneous media with a single-exponential decay, the intensity form of Stern–Volmer equation with dynamic quenching is described as follows [19].

$$I_0/I = 1 + K_{SV}[O_2] \quad (1)$$

where I is luminescent intensity. The subscript 0 denotes a value in the absence of quencher, K_{SV} is the Stern–Volmer constant, and $[O_2]$ is O_2 concentration. A plot of I_0/I versus $[O_2]$ should be linear with identical slopes of K_{SV}. However, all the Stern–Volmer plots are nonlinear, which means that the microenvironments around $[Cu(TBT)(POP)]BF_4$ molecules are inhomogeneous, and thus the quenching behavior within the four samples should not be described by Expression 1. As mentioned earlier, the samples are uniform and homogeneous, which means that the inhomogeneous microenvironments are caused by the probe molecules themselves.

According to Li's report, in a hydrophobic environment, all $[Cu(N–N)(P–P)]^+$ complexes with π surfaces tend to form a dual-molecule structure, where N–N and P–P stand for diimine and phosphorous ligands [20]. With the formation of this dual-molecule structure, two molecules are bonded head-to-head (the diimine moiety is defined as the "head"), resulting in a somewhat rigid structure and consequently suppressed geometric relaxation. Considering the large π surface of TBT and the hydrophobicity matrix of polystyrene, we believe $[Cu(TBT)(POP)]BF_4$ molecules also experience this kind of intermolecular aggregation, leading to the inhomogeneous microenvironments. In this case, we assume that there are two primary luminophore

Table 4 Values of sensitivity and nonlinear fitting results of the four samples

Sample	I_0/I_{100}	K_{SV1} ($O_2\%^{-1}$)	K_{SV2} ($O_2\%^{-1}$)	f_1	f_2	R^2
1 wt% doped	5.1	0.2087	0.0034	0.783	0.217	0.9993
1.5 wt% doped	5.5	0.2201	0.0009	0.834	0.166	0.9993
2 wt% doped	5.8	0.2092	0.0023	0.827	0.173	0.9996
2.5 wt% doped	4.4	0.1485	0.0023	0.783	0.217	0.9993

sites in the matrix, mono-molecule and dual-molecule sites, and the Stern–Volmer equation should be described as:

$$\frac{I_0}{I} = \frac{1}{\frac{f_1}{1+K_{SV1}pO_2} + \frac{f_2}{1+K_{SV2}pO_2}} \quad (2)$$

where f_1 and f_2 are the fractional contributions from each oxygen accessible site ($f_1 + f_2 = 1$), K_{SV1} and K_{SV2} are the associated Stern–Volmer quenching constants for each oxygen accessible site [19]. The nonlinear fitting results are summarized in Table 4 and shown in Fig. 5. It can be observed that the two-site model is applicable for the four samples, confirming the correctness of our hypothesis that the inhomogeneous microenvironments are caused by the probe molecules themselves.

Response/recovery properties and photostability of [Cu(TBT)(POP)]BF_4/polystyrene nanofibrous membranes

The inset of Fig. 5 demonstrates the PL intensity responses of the 2 wt% doped sample when exposed to periodically varied 100% N_2 and 100% O_2 atmospheres. Here, we define 95% response time as the time taken for a sample to lose 95% of its initial emission intensity when changed from 100% N_2 atmosphere to 100% O_2 atmosphere, and 95% recovery time as the time taken to recover 95% if its final emission intensity when changed from 100% O_2 atmosphere to 100% N_2 atmosphere. Correspondingly, the 2 wt% doped sample renders a response time of only 5 s and a recovery time of 13 s. The quick response toward O_2 and N_2 suggests that the 2 wt% doped sample is highly sensitive toward O_2, and we attribute the quick response character to the large surface-area-to-volume ratio of nanofibrous membranes. In addition, the recovery time is obviously longer than the response time, which can be explained by the diffusion-controlled dynamic response and recovery behavior of a hyperbolic-type sensor reported by Mills and coworkers [21]. The 2 wt% doped sample renders a good photostability by showing no obvious photobleaching.

Conclusion

In this paper, we report the synthesis, crystal structure, photophysical properties, and electronic nature of a phosphorescent Cu(I) complex of [Cu(TBT)(POP)]BF_4. We fabricated electrospinning composite nanofibers of [Cu(TBT)(POP)]BF_4 and polystyrene, hoping to explore the possibility of replacing precious-metal-based oxygen sensors with cheap Cu-based ones. The resulted samples exhibit a maximum sensitivity of 5.8 toward oxygen with short response/recovery time due to the large surface-area-to-volume ratio of nanofibrous membranes, and no photobleaching is detected in these samples. All these results suggest that phosphorescent Cu(I) complexes doped on nanofibrous membranes are promising candidates for low-cost and quick-response oxygen-sensing materials.

Acknowledgments The authors gratefully thank the financial and experimental supports from Beijing Institute of Genomics, Chinese Academy of Sciences.

References

1. Erkkila KES, Odom DT, Barton JK (1999) Chem Rev 99:2777
2. Bignozzi CA, Argazzi R, Kleverlaan CJ (2000) Chem Soc Rev 29:87
3. McMillin DR, McNett KM (1998) Chem Rev 98:1201
4. Armaroli N (2001) Chem Soc Rev 30:113
5. Eggleston K, McMillin DR, Koenig KS, Pallenberg AJ (1997) Inorg Chem 36:172
6. Cunningham T, Cunningham KLH, Michalec JF, McMillin DR (1999) Inorg Chem 38:4388
7. Cuttell DG, Kuang SM, Fanwick PE, McMillin DR, Walton RA (2002) J Am Chem Soc 124:6
8. Rader RA, McMillin D, Buckner MT, Matthews TG, Casadonte DJ, Lengel RK, Whittaker SB, Darmon LM, Lytle FE (1981) J Am Chem Soc 103:5906
9. Rader RA, McMillin D, Buckner MT, Matthews TG, Casadonte DJ, Lengel RK, Whittaker SB, Darmon LM, Lytle FE (1981) J Am Chem Soc 103:5906
10. Palmer EA, McMillin DR (1987) Inorg Chem 26:3837
11. Zhang Q, Zhou Q, Cheng Y, Wang L, Ma D, Jing X, Wang F (2004) Adv Mater 16:432
12. Yang L, Feng JK, Ren AM, Zhang M, Ma YG, Liu XD (2005) Eur J Inorg Chem 10:1867
13. Lei B, Li B, Zhang H, Zhang L, Li W (2007) J Phys Chem C 111:11291
14. Vander Tol EB, Van Tamesdonk HJ, Verhoeven JW, Steemers FJ, Kerver EG, Verboom W, Reinhoudt DN (1998) Chem Eur J 4:2315
15. Kranenburg M, Van der Brugt YEM, Kamer PCJ, Van Leeuwen PWNM (1995) Organometallics 14:3081
16. Yoon J, Cha SK, Kim JM (2007) J Am Chem Soc 129:3038
17. Wang Y, Li B, Liu Y, Zhang L, Zuo Q, Shi L, Su Z (2009) Chem Commun 39:5868
18. Wang X, Drew C, Lee SH, Senecal KJ, Kumar J, Samuelson LA (2002) Nano Lett 2:1273
19. Shi L, Lu S, Zhu D, Li W (2009) Appl Organomet Chem 23:379
20. Zhang L, Li B, Su Z (2009) Langmuir 25:2068
21. Mills A, Lepre A (1997) Anal Chem 69:4653